Multi-objective Risk Analysis for Crowd Evacuation Guidance using Multiple Visual Signs

Akira Tsurushima[a]
Intelligent Systems Laboratory, SECOM CO., LTD., Mitaka, Tokyo, Japan

Keywords: Evolutionary Multi-objective Optimization, Black-box Optimization, Visual Evacuation Signage Assignment Problem, Average Value at Risk, NSGA-II.

Abstract: Efficient crowd evacuation guidance is crucial but challenging owing to the randomness involved in evacuation situations and to the unpredictable human behaviors, e.g., herd behavior among evacuees. Many researchers have found that visual evacuation signage is useful for this purpose, and, thus, evacuation guidance systems employing visual signage have been developed. A proper arrangement of visual signs on the premises is necessary to obtain the most out of these attempts; however, several factors make this task challenging, such as multiple conflicting objectives in the evacuations and randomness and uncertainties in the situation. This study formulates the visual evacuation signage assignment problem as a stochastic multi-objective optimization problem and explores the efficient layouts of multiple visual signs on the premises. We consider two objectives for the efficient layout of visual signs, namely, maximizing the number of evacuees selecting the correct exit and minimizing the total evacuation time. The average value at risk is employed to deal with the risks involved in noisy objective functions, while the expected values of these objectives are optimized. Pareto-optimal solutions satisfying both the expected values and the risk measures were explored in cases with one, two and five evacuation signs using the NSGA-II algorithm.

1 INTRODUCTION

Numerous researchers have found that cognitive factors during evacuations are crucial because they often make individual behaviors uncertain and sometimes lead to unexpected crowd behaviors (Haghani, 2020b; Haghani, 2020a). Herd behavior, i.e., the tendency of an individual to follow other people's behaviors or decisions, is one of those still unclear, albeit well-studied, cognitive factors in crowd evacuations (Haghani et al., 2016; Sieben et al., 2017). One difficulty caused by herd behaviors in evacuations is the large variances of the results, which make the consequences of the evacuation protocol designs unpredictable. This is especially true if the evacuation process involves some evacuation decisions, such as selections of the evacuation routes or exits, or choices of evacuation actions (Haghani and Sarvi, 2016; Lovreglio et al., 2014). Unsymmetry in exit choices in crowd evacuations is a well-known example of unpredictable crowd evacuation behavior (Helbing et al., 2000; Ji et al., 2017; Tsurushima, 2019; Tsurushima, 2020; Tsurushima, 2021a).

Recently, evacuation protocols employing visual signs or signage systems to achieve efficient evacuations have been designed and developed (Galea et al., 2014; Zhou et al., 2019). The proper arrangement of visual signs within the premises is crucial in these attempts; simulations and optimization techniques are often employed to explore the efficient positions of visual signs (Cisek and Kapalka, 2014; Dubey et al., 2020). However, several properties of the problem make this task challenging, e.g., large decision spaces, computationally expensive evaluation methods, noisy objective functions, lack of efficient search methods, and multiple conflicting objectives. These factors result in high computational costs that are often unaffordable for most architectural projects.

Tsurushima addressed these issues in the visual signage arrangement problem for crowd evacuations and formulated it as a stochastic multi-objective optimization problem, namely, the visual evacuation signage assignment problem (VESAP) (Tsurushima, 2021c). Tsurushima analyzed an instance of the VESAP in which evacuees must choose one of two exits— the correct (safe) exit and the incorrect one — to flee from the environment. The problem has two

[a] https://orcid.org/0000-0003-2711-297X

Tsurushima, A.
Multi-objective Risk Analysis for Crowd Evacuation Guidance using Multiple Visual Signs.
DOI: 10.5220/0010886400003116
In *Proceedings of the 14th International Conference on Agents and Artificial Intelligence (ICAART 2022) - Volume 1*, pages 71-82
ISBN: 978-989-758-547-0; ISSN: 2184-433X

objective functions: the number of evacuees selecting the correct exit f_1 (to be maximized) and the total evacuation time of the crowd f_2 (to be minimized). Objective f_2 is crucial because the single objective problem with f_1 will lead to an optimal solution: a position in front of the incorrect exit. In this solution, many evacuees move to the incorrect exit first and then change to the correct one, leading to an unnecessarily long travel distance, which also leads to a long evacuation time.

Tsurushima considered the VESAP as the mean risk model and analyzed it in terms of the Pareto-efficiencies and risks associated with the solutions. However, in his analysis, he only considered a single visual sign assignment case that might be considered unrealistic in practice. He also assumed a discrete decision space and conducted brute-force approaches for all the candidate positions of assigning the visual sign to analyze the Pareto-optimal solutions, which might be inapplicable to practical problems, owing to the computational cost.

In this study, we analyzed the VESAP in cases with multiple visual signs. The combinatorial property of the problem leads to a large decision space and costly computations, making the brute-force approach inapplicable. Assuming a continuous search space, we applied multiple objective optimization techniques to explore the Pareto-frontiers and employed the average value at risk to estimate the risks involved in the solutions.

2 MOTIVATING EXAMPLE AND BASIC CONCEPT

Figure 1 shows the means of three example solutions, p_1, p_2, and p_3, of the VESAP on the objective space of f_1 and f_2, indicated in black, green, and red, respectively. Because f_1 is to be maximized and f_2 is to be minimized, the solutions close to the lower-right corner are preferable, whereas those close to the upper-left corner are not. Twenty-four simulations were conducted for each solution, and the objective values of each Realization were plotted as '$\times$' on the objective space. Realizations of each solution are broadly distributed over the objective space, owing to the effects of herd behaviors and to the random properties of the problem. This makes it difficult to specify the coordinates of the points that properly represent the outcomes of the solutions on the objective space. One possible way to represent the solutions is to use the expected values of the objective functions $(\bar{f}_1, \bar{f}_2)$ by explicit sampling, which are shown in small filled circles in Fig. 1. This approach has been employed to

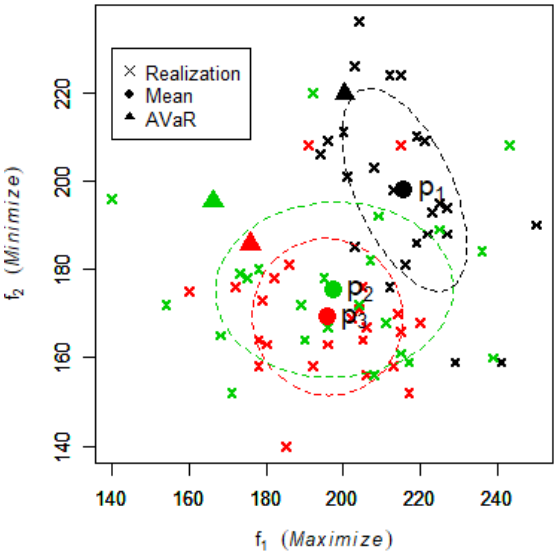

Figure 1: Motivating example.

solve many stochastic optimization problems; however, it disregards the risk or uncertainty involved in the problem, i.e., solutions with large and small variances are indistinguishable.

Most human decision makers tend to avoid risks, meaning that they have concave utility functions. People prefer random variables with a small variance to those with a large one if the expected values are equal. Thus, the quantities to be maximized are not the expected values, but rather are their expected utilities. However, in general, estimating people's utility functions is difficult or sometimes impossible.

In Fig. 1, the expected values of the objective functions of p_2 and p_3 are close to each other for both f_1 and f_2; thus, two solutions are almost indistinguishable if we only consider the expected values. The ellipses in Fig. 1 illustrate the 50% probability ellipses of three solutions, i.e., the ranges where 50% of those Realizations will fall within. In the figure, the probability ellipse of p_2 is larger than that of p_3 and almost includes the ellipse of p_3. This implies that the outcomes of p_2 are more unpredictable than those of p_3, even though the expected values are almost equal; human decision makers usually prefer p_3 to p_2 because most people are averse to risk and dislike unpredictability. Because risks are major factors in evacuation problems, the risk attitude of decision makers is crucial and should be considered in the evacuation protocol analysis. Some numerical risk measures that properly represent risks in the solutions would be desirable.

The average value at risk (AVaR), which is a widely used risk measure in many fields, including economics and finance, is currently considered

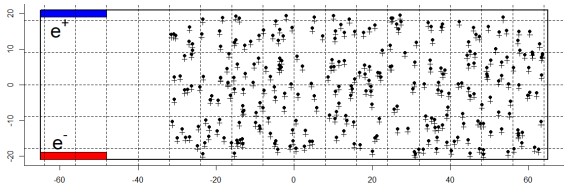

Figure 2: S_1: e^+ and e^- are indicated in blue and red, respectively. The intersections of the dashed lines indicate the candidate positions.

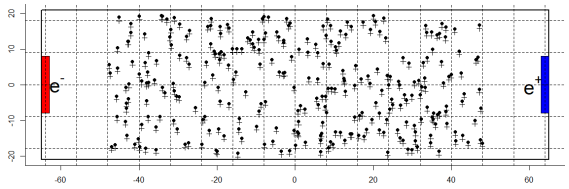

Figure 3: S_2: e^+ and e^- are indicated in blue and red, respectively. The intersections of the dashed lines indicate the candidate positions.

a coherent risk measure that is consistent with the maximum expected utility principle and second-order stochastic dominance (Gutjahr and Pichler, 2016; Ogryczak and Ruszczynski, 2002). The AVaR also satisfies several desired properties, including monotonicity, positive homogeneity, subadditivity, and translation invariance. It is defined on the basis of the value at risk (VaR), which is another risk measure employed prior to the AVaR (Rachec et al., 2008).

Definition 1 (Value at Risk: VaR)**.** *The value at risk of the random outcome X at level $\alpha(0 < \alpha \leq 1)$ is the $\alpha-$quantile[†] of the random variable X, i.e.,*

$$VaR_\alpha(X) = F_X^{-1}(\alpha).$$

Definition 2 (Average Value at Risk: AVaR)**.** *The AVaR of the random outcome X at level $\alpha(0 < \alpha \leq 1)$ is defined[†] as*

$$AVaR_\alpha(X) = \frac{1}{\alpha}\int_0^\alpha VaR_p(X)dp \quad (1)$$
$$= \mathbf{E}[X|X \leq VaR_\alpha(X)]. \quad (2)$$

The triangles in Fig. 1 depict the coordinates of $(AVaR_{0.3}(f_1), AVaR_{0.3}(f_2))$ of p_1, p_2, and p_3 in black, red, and green, respectively.

In Fig. 1, it is difficult or impossible to set the order of the expected values of p_1, p_2, and p_3 (three filled circles) without using someone's subjective preferences because one may have a better value for one objective function than those of the others while having a worse value for another objective function. Solutions like these are called Pareto-optimal in multi-objective optimizations (Gutjahr and Pichler, 2016).

Definition 3 (Pareto-optimal)**.** *A solution x is said to be non-dominated, Pareto-efficient, or Pareto-optimal if no solution $y \neq x$ dominates x. A solution y is said to dominate x if a solution y satisfies the following:*[‡]

1. $\forall h : f_h(y) \geq f_j(x)$
2. $\exists g : f_g(y) > f_g(x)$.

If x is a Pareto-optimal solution, the image of x, $f(x)$, is called the Pareto-optimal point and the set of Pareto-optimal points on the objective space is called the Pareto-frontier.

In our example, p_2 and p_3 are Pareto-optimal points with respect to the expected values; however, p_2 is dominated by p_3 with respect to the risks because p_3 has better values for both $AVaR_{0.3}(f_1)$ and $AVaR_{0.3}(f_2)$ than those of p_2. By considering AVaRs, we may conclude that p_3 is a better solution than p_2 because p_3 has smaller risks than those of p_2, even though the expected values of the two are almost equivalent.

3 VISUAL EVACUATION SIGNAGE ASSIGNMENT PROBLEM

In the VESAP, 300 agents $A = \{a_1, \ldots, a_{300}\}$ are randomly distributed on the two-dimensional Euclidian space $S \in \mathbb{R}^2$; S has two exits: the correct exit e^+ and the incorrect exit e^- for the agents to flee from the space. The correct exit is assumed to lead the agents to safe evacuations; thus, the aim of the problem is to maximize the number of agents who select e^+. In addition, another objective, the total evacuation time, is introduced to the VESAP because a single objective problem with f_1 will lead to a solution that has an unnecessarily long evacuation time, which is a serious problem in most evacuation situations. These objectives were evaluated through multi-agent simulations; the outcomes of the simulation were contaminated with noise owing to the randomness and herd behaviors of the agents. Therefore, Tsurushima (2021b) formulated the VESAP as a stochastic multi-objective problem. In this paper, we adopt a simplified version of the formulation as follows:

[†]In the financial field, VaR is usually defined as the negative α-quantile of the random variable X because X is the return value, which can be negative or positive but not the outcome itself. However, we use this definition (outcome) for simplicity.

[‡]We assumed f_i to be maximized.

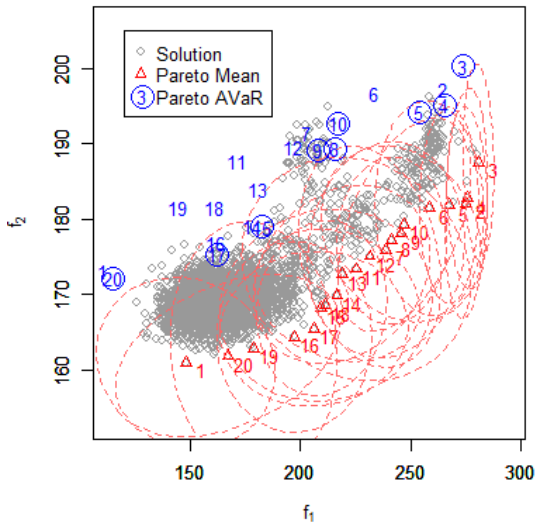

Figure 4: Case study for S_1.

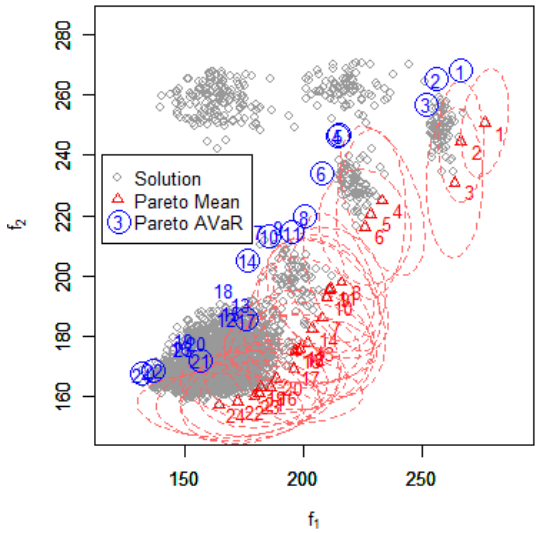

Figure 5: Case study for S_2

$$max \quad f_1(k,\omega) \tag{3}$$
$$max \quad -f_2(k,\omega) \tag{4}$$
$$s.t. \quad k \in \mathcal{K},\ |k| \le L,\ \omega \in \Omega.$$

Here, $k = \{(x,y),\ldots\}$ represents a set of visual sign coordinates on S, $\mathcal{K}$ represents the solution space, L is the maximum number of visual signs assigned to S, ω is a stochastic scenario, and Ω is the sample space. The functions f_1 and f_2 are the two objective functions of the VESAP referring to the number of agents selecting the correct exit and the total evacuation time, respectively. Because we want to minimize the total evacuation time, $-f_2$ is maximized. In this study, we examined two example spaces with different arrangements of exits, S_1 and S_2, as shown in Figs. 2 and 3, respectively. Both S_1 and S_2 are $x \in [-65,65], y \in [-21,21]$ units with different layouts of e^+ (the blue exit) and e^- (the red exit).

Moreover, in this study, we analyzed the VESAP in cases with $L \ge 2$ signs, whereas Tsurushima (2021b) only examined $L = 1$. The evacuation decision model (Tsurushima, 2019), which represents the herd behavior of evacuees, was incorporated into each agent; however, the social force model (Helbing et al., 2000) was not employed owing to the computational cost. We also assumed that the visual field of an agent is a fan shape with a radius of 10 units and an angle of 20° (Tsurushima, 2021b; Tsurushima, 2021d).

4 TWO VISUAL SIGNS: A CASE STUDY

In this section, the VESAP in the case with two visual signs ($|k| = 2$) is examined. We assumed the candidate positions of the visual signs as $x = \{-64, -56, -48, -40, -32, -24, -16, -8, 0, 8, 16, 24, 32, 40, 48, 56, 64\}$ and $y = \{-18, -9, 0, 9, 18\}$; a total of 85 candidate positions were introduced on S. We conducted 24 simulation runs for each assignment of the visual signs using a combination of two out of 85 candidate positions (3570 combinations) for S_1 and S_2.

Figures 4 and 5 show the results of the simulations for S_1 and S_2, respectively. Because we want to maximize f_1 and minimize f_2, the lower-right corner of the figure is the best position and the upper-left one is the worst position of these spaces. The gray small circles show the means of f_1 and f_2 for all solutions (3570 combinations of the candidate positions), and the red triangles with numbers indicate the Pareto-optimum of those solutions. The blue numbers depict the AVaRs of f_1 and f_2 associated with the Pareto-optimal solutions; the blue numbers with a blue circle indicate that these points are the Pareto-optimal for the AVaR.

5 METHOD

In Section 4, we assumed 85 candidate positions and assigned visual signs to any of two positions. We examined a total of 3570 ($_{85}C_2$) feasible combinations through simulations. A total of 24 simulations were conducted for each feasible solution to estimate the means of f_1 and f_2. Thus, 85,680 simulation trials were performed to obtain the Pareto-optima. However, this type of brute-force approach is unrealistic and inapplicable in general cases due to the high computational cost; for example, 2,370,480 simulations will be required with three visual signs. An efficient

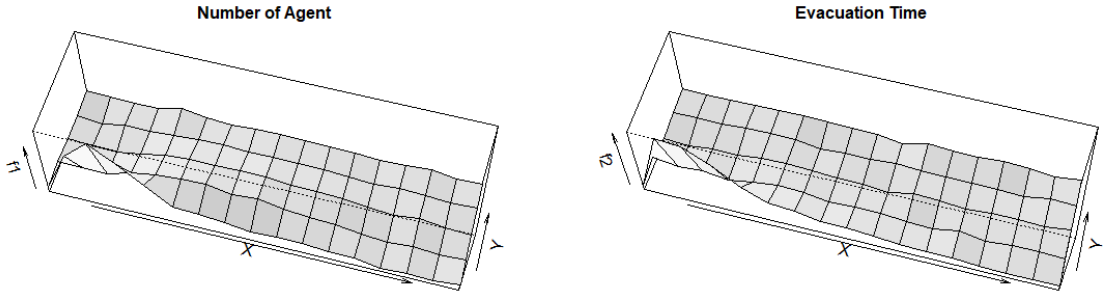

Figure 6: Landscapes of S_1. The left figure shows f_1, and the right figure shows f_2.

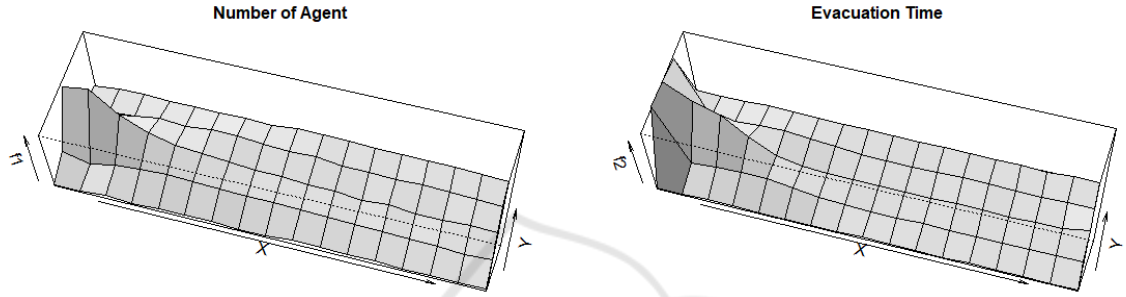

Figure 7: Landscapes of S_2. The left and right figures show f_1 and f_2, respectively.

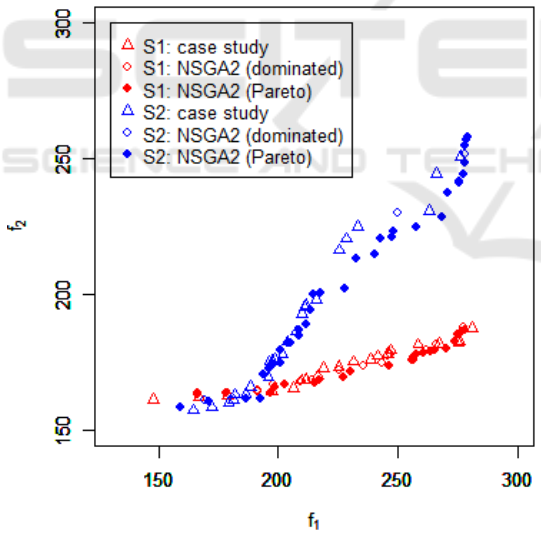

Figure 8: Case study and NSGA (S_1 and S_2).

method to obtain the Pareto-optima is required for the VESAP.

A black-box optimization technique is useful for this purpose. The evolutionary multi-objective optimization (EMO) algorithm is one such technique that is also applicable for multi-objective optimization problems with noisy objective functions. The EMO algorithm is a multi-point search meta-heuristic that holds a set of candidate solutions and gradually converges them to Pareto-frontiers. One advantage of this technique is the ease of implementing it to a parallel algorithm because a set of candidate solutions are mutually independent. In particular, parallel simulations can be applied to evaluate these solutions.

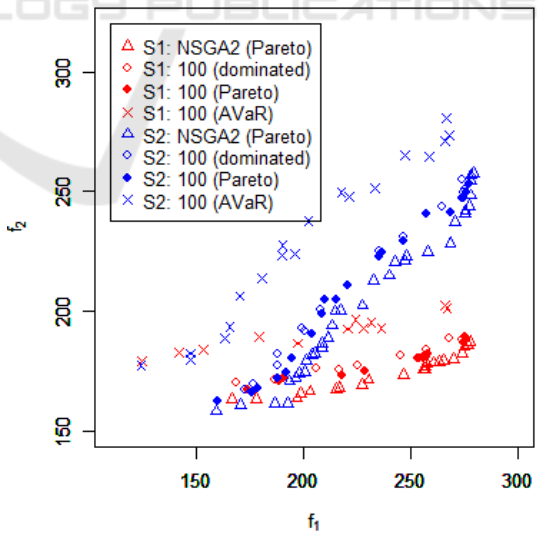

Figure 9: Pareto-optima obtained by NSGA-II and 100 simulations (S_1 and S_2).

Theoretically, the VESAP has four objective functions: the expected values and AVaRs of f_1 and f_2, respectively. However, multi-objective problems with many objectives lead to a large number of Pareto-

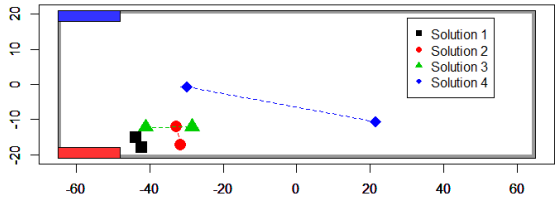

Figure 10: Four representative solutions satisfying the Pareto-optimal for both the expected values and AVaRs for the two-sign case in S_1

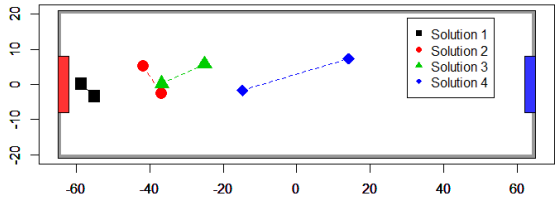

Figure 11: Four representative solutions satisfying the Pareto-optimal for both the expected values and AVaRs for the two-sign case in S_2

optima and are difficult to address. We conducted simulations by assigning a single evacuation sign for each 85 candidate position to examine the landscapes of objective functions f_1 and f_2. The simulations were repeated 250 times, and the mean values of f_1 and f_2 were estimated. Figures 6 and 7 show the landscapes of both objectives for S_1 and S_2, respectively. The left figure depicts the landscape of f_1, and the right figure depicts the landscape of f_2. These figures illustrate that all of the four landscapes were found to be smooth, flat, and not complex. We expect that the problem will be handled by most optimization algorithms.

Tsurushima (2021c) analyzed the correlations between the expected values and the AVaRs, and found that these two are highly correlated for both f_1 and f_2 (Observation 8 in (Tsurushima, 2021c)). This observation suggests that VESAP can be reduced to a bi-objective optimization problem, which is easier to handle than the four-objective problem, with the expected values of f_1 and f_2. Because the expected values and AVaRs are highly correlated, AVaRs of f_1 and f_2 may be treated after the expected values of the Pareto-optima of f_1 and f_2 were obtained.

NSGA-II (Deb et al., 2002) is one of the most representative and widely applied evolutionary algorithms for solving multi-objective optimization problems. The fast non-dominated sort algorithm in NSGA-II can efficiently generate a series of ranked non-dominated frontiers with $O(MN^2)$ computational complexity. Here, N is the population size, and M is the number of objectives. Crowding distances are also used in NSGA-II to keep individuals in a population diverse to represent the entire Pareto-frontier properly. NSGA-II is known as a good algorithm for a problem with a relatively small number of objective functions.

In this study, we formulated VESAP as a bi-objective optimization problem with the expected values of f_1 and f_2 as the objective functions. Then, we employed the NSGA-II algorithm to obtain a set of Pareto-optimal solutions for a bi-objective problem. Because the outcome of a solution is evaluated through a simulation, numerous simulation trials are required to estimate the expected values. Determining the number of simulations to estimate an expected value is debatable because the solutions will be untrusted if the number is small, whereas it is accurate but computationally expensive if the number is large. We conducted 24 simulations, similar to that in Section 4, to estimate the expected values for each solution in the NSGA-II search procedure. Thus, to obtain a set of Pareto-optima, we required a total of $24NG$ simulations in a single NSGA-II run with N population size and G generations.

However, the number 24 might be quite small to explore a Pareto-optimum that is precise to represent the true Pareto-frontiers. Therefore, we adopted a two-phase approach. First, we explored a set of Pareto-optima using NSGA-II with a small number (N=24) of simulations. Second, 100 simulation runs were reconducted for the Pareto-optima obtained in the first phase to calculate more accurate expected values and AVaRs. Note that some Pareto-optima obtained in the first phase might degenerate in the second phase.

In this study, *NetLogo 6.0.2* (Wilensky, 1999) was used to implement the crowd evacuation simulator by using the evacuation decision model. The entire procedure was implemented in *R x64 3.5.1* with the following libraries: *nsga2R* for the NSGA-II algorithm, *parallel* for the parallel execution of the simulations and *RNetLogo* for the connection between *R* and *NetLogo*. Simulations and optimizations were executed on a machine with an *Intel Core i7-6700* CPU.

6 PERFORMANCE ANALYSIS

6.1 Case Study and NSGA-II

First, we attempted to explore the Pareto-optimal solutions for the case with two visual evacuation signs like in Section 4. The coordinates of the visual signs were chosen as continuous decision Variables, $x \in [-65, 65]$ and $y \in [-21, 21]$, and the NSGA-II algorithm with 36 populations and 50 generations was ap-

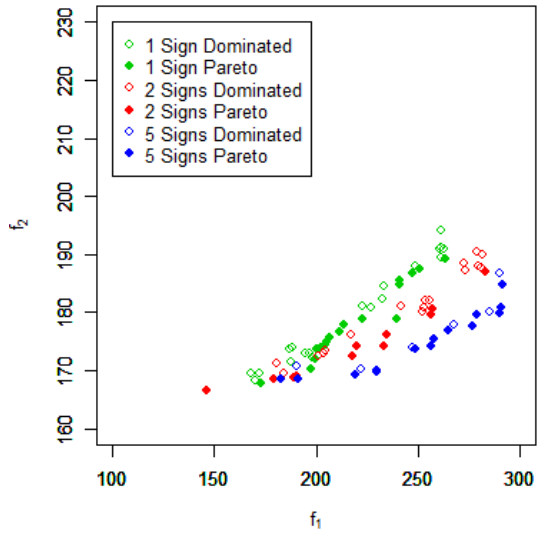

Figure 12: Expected value of the Pareto-frontier for S_1. The one-, two-, and five-sign cases are depicted in green, red, and blue, respectively.

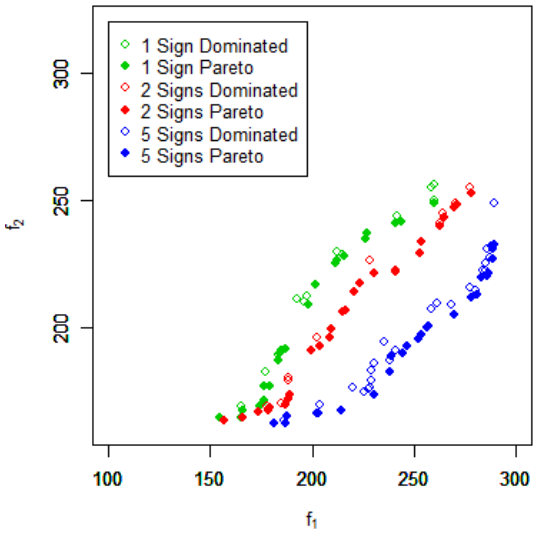

Figure 14: Expected value of the Pareto-frontier for S_2. The one-, two-, and five-sign cases are depicted in green, red, and blue, respectively.

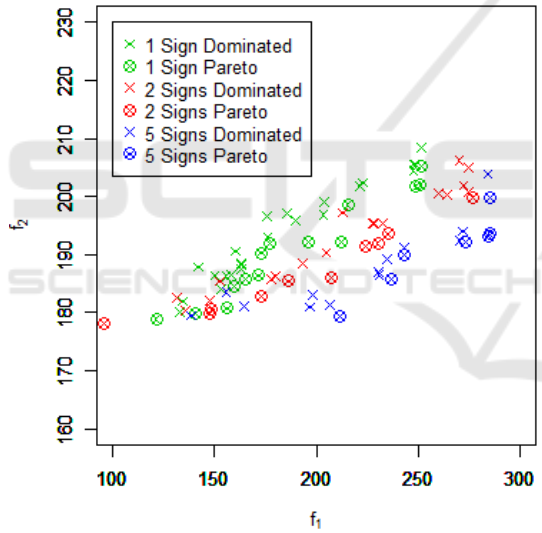

Figure 13: AVaR of the Pareto-frontier for S_1. The one-, two-, and five-sign cases are depicted in green, red, and blue, respectively.

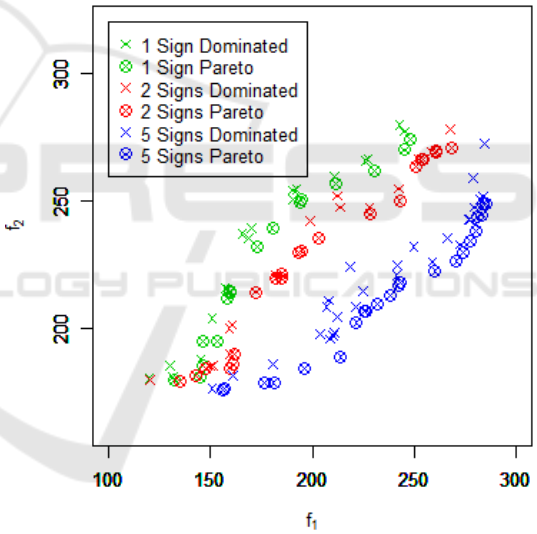

Figure 15: AVaR of the Pareto-frontier for S_2. The one-, two-, and five-sign cases are depicted in green, red, and blue, respectively.

plied to explore the Pareto-optima. Because 24 simulations were repeated to estimate the expected values of f_1 and f_2 for each solution, a total of 43,200 simulations were performed to obtain the Pareto-optimal solutions.

Figure 8 shows the results of NSGA-II with the results obtained in the case study presented in Section 4 for S_1 and S_2. The red triangles show the Pareto-optima obtained by the brute-force approach in Section 4; the blue open and filled circles represent the dominated and the Pareto-optimal solutions obtained by NSGA-II, respectively. NSGA-II explored 22 and 36 Pareto-optimal solutions for S_1 and S_2, respectively. These figures show that the Pareto-optima obtained by NSGA-II almost overlap with those obtained by the brute-force approach, even though the former only requires 43,200 simulations, whereas the latter requires 85,680 simulations. This shows that NSGA-II can explore Pareto-optima reasonably good enough with lower computational cost.

Table 1: Four representative solutions satisfying the Pareto-optimal for both the expected values and the AVaRs in the two-sign case.

Solution		$\bar{f}_1$	$\bar{f}_2$	$AVaR(f_1)$	$AVaR(f_2)$
S_1	1	274.67	186.63	267.07	201.33
	2	257.40	180.92	236.40	192.80
	3	217.98	173.04	197.37	186.50
	4	173.97	167.38	124.63	178.93
S_2	1	276.43	249.65	267.93	273.40
	2	220.80	210.91	202.23	237.73
	3	203.74	190.28	180.63	213.77
	4	175.62	166.07	147.10	179.50

6.2 Validation Simulation

We then reconducted 100 simulation runs for the Pareto-optima obtained by NSGA-II to evaluate the expected values and AVaRs accurately. Figure 9 shows the Pareto-optimal solutions obtained by NSGA-II and the results of 100 simulations reconducted for the validation purpose. The black filled circles show the Pareto-optima obtained by NSGA-II, and the red filled and open circles show the Pareto-optimal and the dominated solutions obtained by 100 simulations, respectively. The AVaRs at level 0.3 of these Pareto-optima are also indicated by the red '$\times$' in the figure. In both figures, the red filled circles are located in the upper-left area of the black filled circles, suggesting that NSGA-II with 24 simulation trials will produce Pareto-optima that are more optimized than the real ones. The numbers of Pareto-optima for S_1 and S_2 decreased to 12 and 19, respectively, in this analysis (red filled circles in Fig. 9). Among these, 8 and 14 solutions in S_1 and S_2, respectively, satisfy the Pareto-efficiency for both the expected values and the AVaRs. Four representative solutions for S_1 and S_2 are presented in Table 1 and illustrated in Figs. 10 and 11, respectively.

6.3 Number of Visual Signs

We also conducted the same analysis for the cases with one, two, and five visual signs to illustrate the effect of the number of visual signs. In the one- and two-sign cases, the population size and the generations in NSGA-II were set to 48 and 50, respectively. In the five-sign case, both the population size and the generations were set to 100. The one-sign case can be considered as a baseline. The one-, two-, and five-sign cases are shown in green, red, and blue, respectively, in Fig. 12 for S_1 and in Fig. 14 for S_2, respectively. The Pareto-frontiers in blue, red, and green are arranged in the order close to the lower right corner, showing that the best result was obtained by the five-sign case and the worst result by the one-sign case.

Table 2: Summary of the analysis in Section 6 for S_1 and S_2. The column labels represent the following: *S*, number of signs; *Pops*, population size in NSGA-II; *Pareto*, number of expected values of the Pareto-optima found in NSGA-II; *EP*, number of expected values of the Pareto-optima; *AP*, number of AVaRs of the Pareto-optima; *EP&AP*, number of expected values and AVaRs of the Pareto-optima. *EP*, *AP*, and *EP&AP* are the results of 100 simulations reconducted on the basis of the Pareto-optima found in NSGA-II (the column labeled *Pareto*).

	S	Pops	Pareto	EP	AP	EP&AP
S_1	1	48	37	17	14	10
	2	48	28	11	10	8
	5	100	20	13	7	6
S_2	1	48	34	22	16	15
	2	48	36	26	21	18
	5	100	49	24	22	18

Table 3: Four representative solutions satisfying the Pareto-optimal for both the expected values and the AVaRs in the five-sign case.

Solution		$\bar{f}_1$	$\bar{f}_2$	$AVaR(f_1)$	$AVaR(f_2)$
S_1	1	291.73	184.73	285.53	199.77
	2	265.12	176.99	243.37	189.97
	3	256.74	174.23	236.87	185.83
	4	229.66	169.82	211.50	179.40
S_2	1	288.80	230.47	283.87	248.60
	2	270.09	204.85	260.40	222.33
	3	230.21	173.12	214.00	188.53
	4	187.04	162.09	155.87	175.37

The AVaRs corresponding to the expected values of the Pareto-optima are presented in Figs. 13 and 15 for S_1 and S_2, respectively. These AVaRs are not necessarily Pareto-optimal, even though the corresponding expected values are. The solutions satisfying the Pareto-optimal for both the expected values and the AVaRs are depicted by '$\otimes$' in Figs. 13 and 15. These solutions are considered to be some of the best solutions to the VESAP because they are Pareto-optima for the expected values and have small risks. The results of the analysis are summarized in Table 2.

Four representative solutions with five signs for S_1 and S_2 are presented in Table 3 and illustrated in Figs. 16 and 17, respectively.

6.4 Illustrative Example

Figures 18 and 19 show two example solutions, P1 and P2, obtained by the VESAP with two visual signs for S_1 in the objective and decision spaces, respectively; Table 4 summarizes these solutions. These example solutions highlight the advantage of the AVaR.

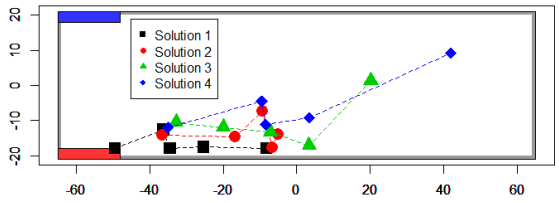

Figure 16: Four representative solutions satisfying the Pareto-optimal for both the expected values and the AVaRs for the five-sign case in S_1.

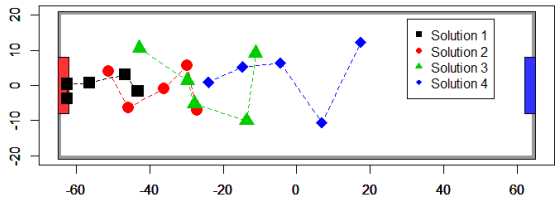

Figure 17: Four representative solutions satisfying the Pareto-optimal for both the expected values and the AVaRs for the five-sign case in S_2.

Table 4: Two example solutions: P1 and P2. The column 'PO' indicates *yes* if the solution is Pareto-optimal for the AVaR; *no* otherwise. A cell with a blue background shows a better value.

	$\bar{f}_1$	$\bar{f}_2$	$AVaR(f_1)$	$AVaR(f_2)$	PO
P1	257.40	180.92	236.40	192.80	*yes*
P2	258.30	181.79	224.33	196.60	*no*

In Fig. 18, the expected values, $AVaR_{0.3}$s, and Realizations of f_1 and f_2 are depicted by the filled circles, triangles, and '×,' respectively. Both P1 and P2 are Pareto-optimal for the expected values; whereas P1 is a Pareto-optimum, P2 is dominated by P1 for the AVaRs (see the blue cells in Table 4). The two dashed ellipses illustrate the 50% probability ellipses of P1 and P2, which reveals that P2 has more risks than those of P1, whereas the expected values of the two are almost equivalent. This is because the probability ellipse of P1 is included in that of P2. The Realizations of P2 distributed more broadly than those of P1 in Fig. 18, which implies that P2 has a greater chance of producing unexpectedly bad outcomes if we adopt it as a solution.

Moreover, the p-values of the Wilcoxon rank sum test for the statistically significant differences between P1 and P2 for $\bar{f}_1$, $\bar{f}_2$, $AVaR(f_1)$, and $AVaR(f_2)$ were 0.50, 0.68, 0.00, and 0.53, respectively.

Figure 19 depicts P1 and P2 on the decision space. The figure illustrates that these two solutions are similar, almost sharing one position (-31, -17) and with the other positions also being close. This example highlights the advantage of the AVaR in that a subtle difference in the decision space will produce a solution that can reduce the risks significantly.

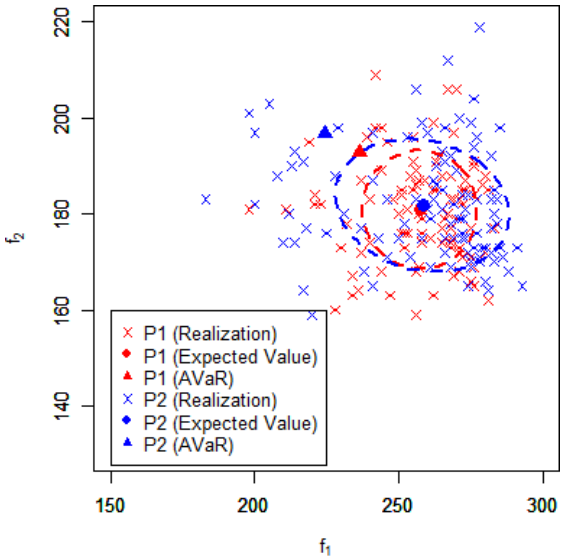

Figure 18: Two example solutions: P1 and P2.

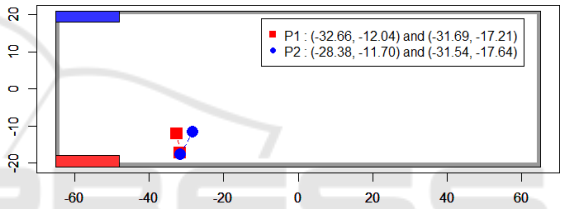

Figure 19: Two example solutions: P1 and P2.

7 RELATED WORKS

Numerous studies have been conducted on multi-objective optimizations, and, currently, many researchers in this field have developed methods that are based on EMO algorithm, which holds a set of solutions, and iteratively approximating them to a Pareto-frontier is intriguing and promising. Some representative EMO algorithms besides NSGA-II include MOEA/D (Zhang and Li, 2007), MSOPS (Hughes, 2005), and NSGA-III (Deb and Jain, 2014). Other approaches promising to solve real-world multi-objective optimization problems with cost-efficient ways are CMA-ES (Hansen and Ostermeier, 1996) and MOTPE (Ozaki et al., 2020).

Numerous works have been conducted to tackle fitness functions contaminated with noise in the EMO. Siegmund et al. (2015) proposed dynamic resampling strategies based on evolutionary generations, Pareto-rankings, and distances to the reference point to mitigate noisy environments (Siegmund et al., 2015). Implicit sampling techniques that use a large population size as a substitute for explicit sampling were proposed in (Tan et al., 2001). Sano and Kita

(2002) proposed a method that has a history of search results to reduce the fitness evaluations (Sano and Kita, 2002). Goh and Tan (2007) adopted an experimental learning-directed perturbation strategy for a noise-tolerant search strategy (Goh and Tan, 2007). Probabilistic dominance was proposed for a robust selection operation against noise in evolutionary optimizations (Fieldsend and Everson, 2005). All of these approaches addressed the issues of how to obtain quality solutions with lower cost; the risks between the real and the expected outcomes, which we addressed in this study, were not considered.

Saadatseresht et al. (2009) formulated a crowd evacuation guidance problem as a multi-objective optimization problem and solved it using NSGA-II to develop evacuation plans (Saadatseresht et al., 2009). Dubey et al. (2020) developed an interactive design support system (AUTOSIGN) to develop an optimal signage system with multiple objectives; the random weight genetic algorithm (MO-RWGA) was applied to handle these objectives in this system (Dubey et al., 2020). Li et al. (2010) developed a method to achieve optimal evacuation route assignments with three objectives, and NSGA-II was employed to solve the problem (Li et al., 2010). However, none of these approaches considered the risks or uncertainties involved in the problem in the solution procedure.

Furthermore, León et al. (2020) analyzed a stochastic multi-objective problem using the AVaR, assuming the risk aversion of the decision makers (León et al., 2020).

8 DISCUSSION

In this study, we analyzed the VESAP with multiple visual evacuation signs from the viewpoint of the expected outcomes and risks involved in the solutions. We formulated the VESAP as a stochastic multi-objective optimization problem with two objective functions: maximizing the number of agents selecting the correct exit (f_1) and minimizing the total evacuation time (f_2). NSGA-II, a multiple objective evolutionary optimization algorithm, was applied to explore the Pareto-optimal solutions, and the Pareto-frontiers of the two objective functions were obtained for the cases with one, two, and five visual signs for two exit layouts (S_1 and S_2). To save computational efforts, we first explored Pareto-optima with a relatively small sampling size (N=24) and then reconducted 100 simulations on the basis of the Pareto-optima obtained by the first trial to produce more accurate results. Solutions satisfying the Pareto-optimal for both the expected values and the AVaRs were obtained in all cases (one, two, and five signs; two layouts: S_1 and S_2).

Figure 8 shows that NSGA-II can explore Pareto-frontiers reasonably close enough to those obtained by brute-force approaches. However, NSGA-II with a small sample size will lead to somewhat inaccurate solutions whose outcomes are estimated optimistically (Fig. 9). This indicates that reconducting simulation with a large sample size may be necessary.

Simulations with a different number of visual signs (Figs. 10, 11, 16, and 17) revealed that having many visual signs always led to better solutions. This is especially true if both the objective values were distant to the extreme point (minimum or maximum). Figure 12–15 show that the difference between the two Pareto-frontiers with a small and a large number of visual signs is significant at the middle of the Pareto-front. If more visual signs are introduced, better solutions would be obtained, whereas the problem with many signs requires massive computational resources. The tradeoff between computational cost and solution quality would be of interest.

We are aware that our research has some limitations and open problems. Some may consider our results inaccurate, owing to the insufficient computational resources. Had we conducted more simulation runs or incorporated the social force model in the simulations, we could have obtained more accurate results. Some approaches that can generate Pareto-optimal solutions with lower costs, as discussed in Section 7, might be adopted for this purpose. We also assumed that the two objective functions are independent and employed a logical conjunction of two AVaRs ($AVaR(f_1) \wedge AVaR(f_2)$) to test the Pareto-efficiency. This might be inappropriate if two objectives are negatively correlated. In such cases, one objective will produce a better outcome, whereas the other will have a worse value; both objectives producing worse outcomes simultaneously will hardly occur though. The logical conjunction of two AVaRs that may overestimate the risks is not likely to realize; a different approach is required to deal with this issue. However, we reserve these problems for future works.

9 CONCLUSION

In this study, we analyzed the VESAP in cases with multiple visual evacuation signs. The NSGA-II algorithm was applied to explore the Pareto-optimal solutions efficiently with a relatively small number of simulation trials. The VESAPs in cases with one, two and five visual evacuation signs were investigated, and the solutions satisfying the Pareto-efficiency for both the

expected values and the AVaRs were obtained for two different exit layouts.

ACKNOWLEDGMENTS

The author is grateful to Mr. Kei Marukawa for helpful discussions and comments on the manuscript. The author would like to thank Editage (www.editage.com) for English language editing.

REFERENCES

Cisek, M. and Kapalka, M. (2014). Evacuation route assessment model for optimization of evacuation in buildings with active dynamic signage system. *Transportation Research Procedia*, 2:541–549. The Conference on Pedestrian and Evacuation Dynamics 2014 (PED 2014), 22-24 October 2014, Delft, The Netherlands.

Deb, K. and Jain, H. (2014). An evolutionary many-objective optimization algorithm using reference-point-based nondominated sorting approach, Part I: Solving problems with box constraints. *IEEE Transactions on Evolutionary Computation*, 18(4):577–601.

Deb, K., Pratap, A., Agarwal, S., and Meyarivan, T. (2002). A fast and elitist multiobjective genetic algorithm: Nsga-ii. *IEEE Transactions on Evolutionary Computation*, 6(2):182–197.

Dubey, R. K., Khoo, W. P., Morad, M. G., Hölscher, C., and Kapadia, M. (2020). AUTOSIGN: A multi-criteria optimization approach to computer aided design of signage layouts in complex buildings. *Computers & Graphics*, 88:13–23.

Fieldsend, J. and Everson, R. (2005). Multi-objective optimisation in the presence of uncertainty. In *2005 IEEE Congress on Evolutionary Computation, IEEE CEC 2005. Proceedings*, volume 1, pages 243–250.

Galea, R. E., Xie, H., and Lawrence, J. P. (2014). Experimental and survey studies on the effectiveness of dynamic signage systems. *Fire Safety Science*, 11:1129–1143.

Goh, C. K. and Tan, K. C. (2007). An investigation on noisy environments in evolutionary multiobjective optimization. *IEEE Transactions on Evolutionary Computation*, 11(3):354–381.

Gutjahr, W. J. and Pichler, A. (2016). Stochastic multi-objective optimization: a survey on non-scalarizing methods. *Annals of Operations Research*, 236(2):475–499.

Haghani, M. (2020a). Empirical methods in pedestrian, crowd and evacuation dynamics: Part I. experimental methods and emerging topics. *Safety Science*, 129:104743.

Haghani, M. (2020b). Empirical methods in pedestrian, crowd and evacuation dynamics: Part II. field methods and controversial topics. *Safety Science*, 129:104760.

Haghani, M. and Sarvi, M. (2016). Human exit choice in crowd built environments: investigating underlying behavioural differences between normal egress and emergency evacuations. *Fire Safety Journal*, 85:1–9.

Haghani, M., Sarvi, M., Shahhoseini, Z., and Bolts, M. (2016). How simple hypothetical-choice experiments can be utilized to learn humans' navigational escape decisions in emergencies. *PLOS ONE*, 11(11):e0166908.

Hansen, N. and Ostermeier, A. (1996). Adapting arbitrary normal mutation distributions in evolution strategies: the covariance matrix adaptation. In *Proceedings of IEEE International Conference on Evolutionary Computation*, pages 312–317.

Helbing, D., Farkas, I., and Vicsek, T. (2000). Simulating dynamical features of escape panic. *Nature*, 407(28):487–490.

Hughes, E. (2005). Evolutionary many-objective optimisation: many once or one many? In *2005 IEEE Congress on Evolutionary Computation*, volume 1, pages 222–227 Vol.1.

Ji, Q., Xin, C., Tang, S., and Huang, J. (2017). Symmetry associated with symmetry break: revisiting ants and humans escaping from multiple-exit rooms. *Physica A*.

León, J., Puerto, J., and Vitoriano, B. (2020). A risk-aversion approach for the multiobjective stochastic programming problem. *Mathematics*, 8(11).

Li, Q., Fang, Z., Li, Q., and Zong, X. (2010). Multiobjective evacuation route assignment model based on genetic algorithm. In *2010 18th International Conference on Geoinformatics*, pages 1–5.

Lovreglio, R., Fonzone, A., dell'Olio, L., and Ibeas, A. (2014). The role of herding behaviour in exit choice during evacuation. *Procedia - Social and Behavioral Sciences*, 160:390–399.

Ogryczak, W. and Ruszczynski, A. (2002). Dual stochastic dominance and related mean-risk models. *SIAM Journal on Optimization*, 13(1):60–78.

Ozaki, Y., Tanigaki, Y., Watanabe, S., and Onishi, M. (2020). Multiobjective tree-structured parzen estimator for computationally expensive optimization problems. In *Proceedings of the 2020 Genetic and Evolutionary Computation Conference*, GECCO '20, page 533–541, New York, NY, USA. Association for Computing Machinery.

Rachec, S. T., Stoyanov, S. V., and Fabozzi, F. J. (2008). *Advanced stochastic Models, Risk Assessment, and Portfolio Optimization: The Ideal Risk, Uncertainty, and Performance Measures*. Wiley.

Saadatseresht, M., Mansourian, A., and Taleai, M. (2009). Evacuation planing using multiobjective evolutionary optimization approach. *European Journal of Operational Research*, 198:305–314.

Sano, Y. and Kita, H. (2002). Optimization of noisy fitness functions by means of genetic algorithms using history of search with test of estimation. In *Proceedings of the 2002 Congress on Evolutionary Computation. CEC'02 (Cat. No.02TH8600)*, volume 1, pages 360–365 vol.1.

Sieben, A., Schumann, J., and Seyfried, A. (2017). Collective phenomena in crowds—where pedestrian dynamics need social psychology. *PLOS ONE*, 12(6):e0177328.

Siegmund, F., Ng, A., and Deb, K. (2015). Hybrid dynamic resampling for guided evolutionary multi-objective optimization. volume 9018.

Tan, K., Lee, T., and Khor, E. (2001). Evolutionary algorithms with dynamic population size and local exploration for multiobjective optimization. *IEEE Transactions on Evolutionary Computation*, 5(6):565–588.

Tsurushima, A. (2019). Modeling herd behavior caused by evacuation decision making using response threshold. In Davidsson, P. and Verhagen, H., editors, *Multi-Agent-Based Simulation XIX. MABS2018. LNAI 11463*, pages 138–152. Springer.

Tsurushima, A. (2020). Validation of evacuation decision model: An attempt to reproduce human evacuation behaviors during the great east japan earthquake. In *In Proceedings of the 12th International Conference on Agents and Artificial Intelligence (ICAART 2020) - Volume 1*, pages 17–27.

Tsurushima, A. (2021a). Herd behavior is sufficient to reproduce human evacuation decisions during the great east japan earthquake. In Rocha, A., Steels, L., and Van den Herik, J., editors, *Agents and Artificial Intelligence. ICAART 2020. Lecture Notes in Computer Science*, volume 12613, pages 3–25. Springer.

Tsurushima, A. (2021b). Reproducing evacuation behaviors of evacuees during the Great East Japan Earthquake using the evacuation decision model with realistic settings. In *Proceedings of the 13th International Conference on Agents and Artificial Intelligence (ICAART 2021) - Volume 1*, pages 17–27. INSTICC, SciTePress.

Tsurushima, A. (2021c). Scochastic multi-objective decision analysis for crowd evacuation guidance using a single visual signage. In *2021 IEEE International Conference on Systems, Man, and Cybernetics (SMC)*, pages 360–367.

Tsurushima, A. (2021d). Simulation analysis of tunnel vision effect in crowd evacuation. In Rutkowski, L., Scherer, R., Korytkowski, M., Pedryca, W., Tadeusiewicz, R., and Zurada, J. M., editors, *Artificial Intelligence and Soft Computing. ICAISC 2021. Lecture Notes in Computer Science*, volume 12854, pages 506–518. Springer.

Wilensky, U. (1999). NetLogo. Center for Connected Learning and Computer-Based Modeling, Northwestern University, Evanston, IL.

Zhang, Q. and Li, H. (2007). MOEA/D: A multiobjective evolutionary algorithm based on decomposition. *IEEE Transactions on Evolutionary Computation*, 11(6):712–731.

Zhou, M., Dong, H., Ioannou, P. A., Zhao, Y., and Wang, F. (2019). Guided crowd evacuation: approaches and challenges. *IEEE/CAA Journal of Automatica Sinica*, 6(5):1081–1094.